RECOVERY AND RECRYSTALLIZATION IN AL ALLOYS FUNDAMENTALS AND PRACTICAL APPLICATIONS

H.J. McQueen* and W. Blum**

*Mech. Eng., Concordia Univ., Montreal, H3G 1M8, Canada
**Mats. Sci., Univ. Erlangen-Nürnberg, Erlangen, Germany

ABSTRACT Recovery and recrystallization play a significant role during mechanical shaping of Al alloys in reducing flow stresses and frequency of defect formation. In thermomechanical processing, they influence product properties through grain size, substructure density and texture; notably, recovery contributes to a balance of high strength and toughness. Dynamic recovery in Al increases gradually through the cold, warm and hot working ranges permitting easy control of effects. The range of equivalent behavior is shifted to higher temperatures as the concentration of solutes and particles increase. Recrystallization is much more sensitive to temperature and alloying and the dynamic form has restricted occurrence in Al alloys. The control of these mechanisms in processes such as extrusion and rolling demand separate consideration.
Keywords: *dynamic recovery, dynamic recrystallization, substructure, extrusion, rolling, static recovery, static recrystallization.*

1. INTRODUCTION

In the primary mechanical forming of Al alloys, dislocation motion is essential for plastic shape change but the levels of tooling forces, frequency of failure and product strength are raised by strain hardening and reduced by restoration mechanisms in either dynamic (D) mode if acting simultaneously with, or in static (S) if acting subsequent to, any stage of straining. To achieve the optimum compromise between a desired increase in shape change (improved productivity) and product strength on one hand and decrease in forces and failure possibility on the other, there needs to be a careful selection of control parameters: temperature T, strain ε and strain rate $\dot{\varepsilon}$ at every stage as well as of T_{ti} and time t_i in intervals between or after the stages [1-6]. The dependence of hardening and restoration mechanisms on these control parameters needs to be established to enhance flexibility, productivity and product quality under industrial conditions.

In Al alloys (grain size ~100 μm), dynamic recovery (DRV) (Figures 1,2) decreases gradually from hot to cold working for strains between 0.5 and 4 as a result of both temperature and stress activation as explained in the next section. The detailed quantitative aspects have been reviewed at ICAA 5 [7,8] and the ideal hot worked state has been described recently [9-11]; in consequence repetition of the details is curtailed. Static recrystallization (SRX) which has been comprehensively reviewed [12,13] is much more commonly utilized practically than dynamic (DRX) which in the high stacking fault energy (SFE) Al alloys occurs under limited conditions as described briefly in Table 1, derived from recent reviews [7-52]. Geometric gDRX (Figures 1,2), serration detachment and rotation rDRX and partial continuous cDRX (as classified by some) are really aspects of high strain DRV as explained before [7,9,10,14,15,21,22,51]. The consideration of grain and subgrain structures will be integrated with microtexture analysis more clearly than before [9,10,19,32,53-57]. The application of these theories will be made to extrusion in which T rises markedly across a narrow deformation zone and to rolling in which T falls gradually during the multistage schedule. Thermomechanical processing, reviewed at ICAA 2 [5,6,58] and control of segregation and particle distribution by homogenization [1,2,5,6,28] are only touched upon.

2. DYNAMIC RECOVERY: HOT, WARM, COLD DEFORMATION

Across the entire range from hot working (T>350°C) to cold working (T<50°C) there is a continuum of dynamic recovery which reduces the dislocation density ρ at the rate:

$$\dot{\rho}^{-} = A\ \rho^{1.5} \exp(-Q/RT) \sinh(b^2 s k_h \sigma/(MkT)) \quad (1)$$

where Q is activation energy for climb, R, the gas constant, b, Burgers vector, s, spacing in walls, k_h, stress concentration factor in walls, k, Boltzmann constant, M, Taylor factor and A, a constant. The rate of generation of dislocations $\dot{\rho}^{+}$ which depends on the strain rate $\dot{\varepsilon}$ and the dislocation density ρ is given by:

$$\dot{\rho}^{+} = (2M/b)\ \dot{\varepsilon}/(c\rho^{-0.5}) \quad (2)$$

where, $c \approx 100$ [59,60]. The net rate of accumulation of dislocations is $\dot{\rho}\ (=\dot{\rho}^{+}-\dot{\rho}^{-})$ giving strain hardening rate $\theta = d\sigma/d\varepsilon = 0.5k'\rho^{-0.5}\dot{\varepsilon}^{-1}\dot{\rho}$ and when integrated over strain 0 to ε_x leads to ρ_x and $\sigma_x = k\rho_x^{0.5}$ (k', constant). Combination of the expressions for $\dot{\rho}^{-}$ and $\dot{\rho}^{+}$ with the condition $\dot{\rho}^{+} = \dot{\rho}^{-}$ for steady state deformation yields the steady state $\sigma - \dot{\varepsilon} - T$ –relation; it is consistent with the experimental data for pure Al if the free parameters are adjusted properly [61]. The evolution of the substructures with ε was described fully at ICAA 5 [7,8].

Considering the flow curves for 400 and 20°C at $\dot{\varepsilon} = 1\ s^{-1}$ for commercial purity Al (<99.99) (Figure 3) σ_s, one can see that, for σ_x at an arbitrary point x in the transient at 400°C, ρ_x is similar at 400 and at 200°C but $\dot{\rho}\left(=\theta 2\rho^{-0.5}\dot{\varepsilon}/k'\right)$ at 20°C is much higher than that at 400°C where $\dot{\rho}^{-}$ is very high due to thermally activated climb. When the strain at 20°C reaches ε_x then in comparison to 400°C, $\rho\left(=\left(\sigma_{20ex}/k\right)^2\right)$ is much higher; hence for 20°C at $\dot{\rho}^{+}$ is much higher and $\dot{\rho}^{-}$ has increased only slightly from that at σ_x due to $\sigma > \sigma_x$ so that $\dot{\rho}$ at 20°C is much higher than $\dot{\rho}$ at

TABLE 1 RESTORATION MECHANISMS IN Al (DEFINITIONS)

MECHANISMS	DYNAMIC (During ε)	STATIC (After ε)
(STRAIN HARDENING) (Dislocation Slip)	Taylor Constraints [7,9,10,13,17,19] Texture Formation	
RECOVERY	DRV [7-11,14-22,43-52] σ monotonically rises under applied strain to become constant in steady state defined by Z.	SRV [12,13,20,23] Gradual decrease in σ, falling substructure stress field declining rate
RECRYSTALLIZATION DISCONTINUOUS	DRX	SRX
	dDRX (Classical) [7,9,10,10,12-16, σ rise to peak, soften 20,33] to steady state only in 99:999+Al at 400°, 280°, 20°C [24-26]	dSRX (Annealing) [12,13] After incubation, rapid soften to completion, rates higher
	In prior cold worked Al [27]	grains finer as T_{def} down ε, $\dot{\varepsilon}$
	In Al-7Mg [21,28-30]	Up, not in steady state [20,21]
		Texture: preferred nucleation, growth [12,13,32]
Particle Stimulated (> 0.6μm)	PSN-dDRX [10,15,21,29,31] Only in Al-5Mg	PSN-dSRX [12,21,34,38,39] Alloys with constituent particles
CONTINUOUS	cDRX [10,15,21,35-37]	cSRX [12,36,42]
Fine Particle (<0.2 μm) Stabilized	After low T TMP, during SPD in supral, Al-l0 Mg,Al-Li [35-37,39]	Very slow almost no growth of cells
Non Stabilized	Warm working, some high ψ walls [10,40,41]	Not in cold working although many high ψ walls [M47,A2]
Partial		
GEOMETRIC	gDRX [7,10,15,21,22,43-49] Pinching off of very thin elongated serrated grains	
Serration Detachment and Rotation	rDRX [10,12,46-50] In Al-Mg alloys meandering serrations pinch-off at base	
GRAIN GROWTH	DGG ($\dot{\varepsilon}$ accelerates) [10,52] In high T, low σ creep	Normal or secondary grain growth [12]

400°C leading to much greater dislocation densities and lower levels of DRV. When steady state ε_s σ_s is reached at 400°C, $\dot{\rho}_s^+ = \dot{\rho}_s^-$ (rate of DRV constant) and $\dot{\rho}_s = 0$ whereas for 20°C at σ_s $\dot{\rho}$ is still high because $\dot{\rho}^-$ is low due to low thermal activation and $\dot{\rho}^+$ is high due to high ρ and for 20°C at ε_s, $\dot{\rho}^-$ has decreased a little compared to $\dot{\rho}^-$ at σ_s due to stress activation but is still high. Ultimately even for 20°C, at very high ε_{s20} σ_{s20}, steady state is also attained; $\dot{\rho}_{s20}^-$ has risen significantly because of stress activation and has become equal to $\dot{\rho}_{s20}^+$ even though ρ_{s20} is very high. In consequence at steady state the rate of DRV $\dot{\rho}_{s20}^-$ is greater than $\dot{\rho}_s^-$ at 400°C because $\dot{\rho}_{s20}^+$ is very high in association with the level of DRV $(\rho_{s20} >> \rho_{s400})$ being much lower at 20°C than at 400°C. This simple analysis is developed into comprehensive analysis by Nes and colleagues [A62,63].

The substructures at high T in the steady state regime $(\varepsilon = 0.2 - 4)$ are relatively simple due to the low σ_s and ρ_s:polygonized subgrains with internal dislocation spacing $\rho^{-0.5}$, constant spacing w of boundaries (SGB) and wall dislocation spacing s [7-11,22,46,47]. While the grains elongate the subgrains remain equiaxed because the SGB are ephemeral or incidental (arising from small local instabilities) and completely rearrange during each $\Delta\varepsilon \approx \varepsilon_s$. The subgrains in a variety of solute and dispersoid alloys are the same size at the same σ_s [7-11,22,46,47]. The "composite" creep model has been successfully formulated to derive the stresses necessary to move dislocations at a uniform rate across the soft grain interior (slowing backstress), and the hard SGB (aiding forward stress), due to the irregular array of dislocations waiting to be incorporated or annihilated [7-10,22,64,65]. In Al, the fairly mobile GB migrate locally to absorb intersecting SGB thus becoming serrated [7,10,14,15,21,22,41,43-48,51,66,67] (Figures 1,2). When the grains elongate becoming very thin, some opposing serrations pinch-off, thus reducing a grain to zero thickness while slowing the thinning of neighboring grains. This process known as gDRX has been found in many alloys, taking place at smaller ε as initial grain size decreases and subgrain size increases (T raised or $\dot{\varepsilon}$ lowered) [15,21,22,43-48].

At 20°C in the range 0.2 to 4, deformation is still in the transient (σ rising) so that dislocations are still being stored in cells that have saturated in size but with ragged walls of rising dislocation density. In this long transient domain with limited annihilation compared to that in steady state hot working, substructure develops with a final aspect ratio of ~2 due to wall elimination in the thinning direction [9,10,19,61,68]. A high fraction of walls become persistent, developing high ψ as ε progresses to produce suitable regions for SRX nucleation [12,13]. In warm working (~250°C), the transient is much shorter (ε_s<4) and the walls appear more recovered than at 20°C but more high ψ walls develop than at 400°C in behavior debatably classed as partial cDRX instead of gDRX [10,40,41,69].

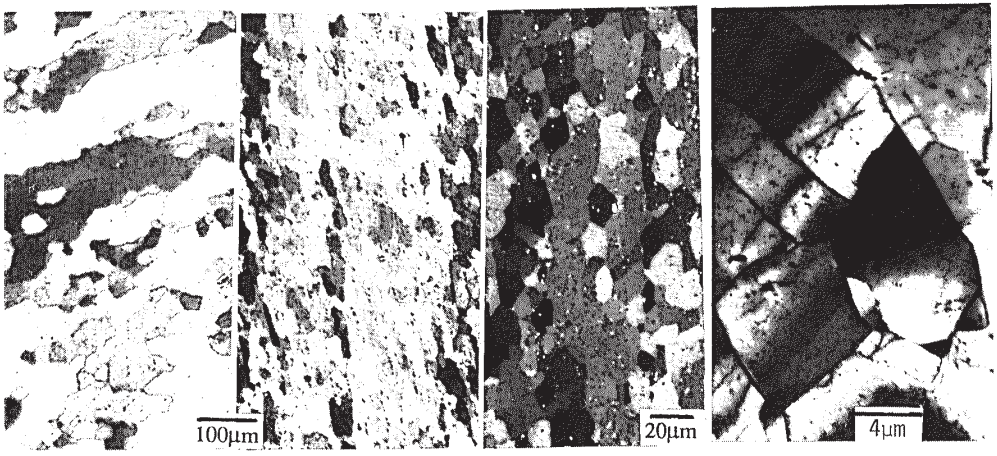

Figure 1. Micrographs of Al deformed in torsion at 400°C, 0.2 s^{-1} to ε=40 (section normal to radius near surface): (a) transition to shoulder illustrating serration formation at ε=2; (a,b) POM 100X, (c) SEM-EBSI and (d) TEM.

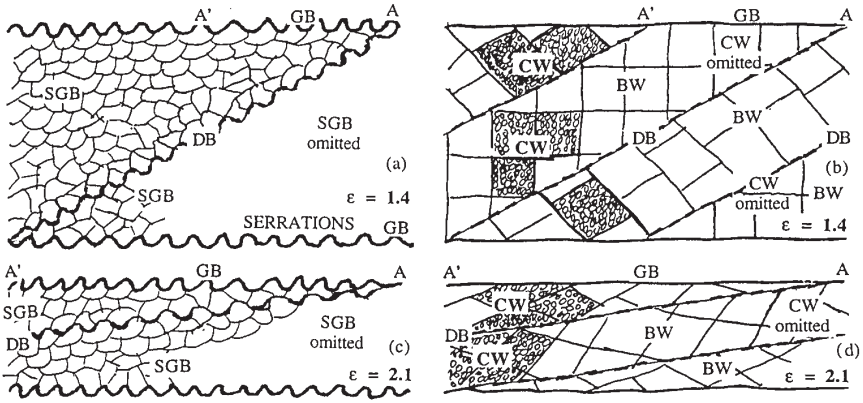

Figure 2. Schematic diagram comparing the hot worked structure (a, b) with subgrain boundaries SGB, disorientation boundaries DB and initial GB, and the cold worked (c, d) with cell walls CW, block wall BW, DB and GB; at two strains ε = 1.4 (a, c) and 2.1 (b, d).

3. SUBSTRUCTURE SCALE , MISORIENTATION AND TEXTURE

The level of DRV was initially characterized by the subgrain size w dependent on T and $\dot{\varepsilon}$ in the steady state regime. An additional visual TEM feature was the regularity of the SGB dislocations; painstaking measurements of dislocation spacing s or misorientations ψ indicated that most were less than 5°. Collected data show that SGB spacing w, internal dislocation spacing $\rho_i^{-0.5}$ and wall spacing s depend uniquely on modulus reduced stress [7-11,19-22,43-45]. The SGB misorientation remained low and independent of strain in steady state, due to the continual rearrangement of the substructure keeping the subgrains equiaxed and the dislocation density and flow stress constant; occasional angles beyond 10° were classed as disorientation boundaries DB or original GB [7-10,19]. Since the visual character of a boundary in TEM and SEM EBSI do not readily specify their misorientation, determination of the ψ distributions of the SGB becomes necessary because they are a significant indication of the level of DRV and the potential for DRX or SRX.

Modern automatic techniques for measuring Kikuchi patterns of every distinct cell, followed by calculation of minimum ψ for every boundary, create maps of all the boundaries with their ψ values[24,40,41,61]. Usually the GB can be discerned by their $\psi \approx$ 20-60° and their continuity; DB can sometimes be similarly traced with $\psi \approx$ 8-20°. The experimental distributions for various purity, heavily worked Al are presented in Figures 4,5 for comparison [24,40,44,61,70,71]. The stable single crystals (<100>, <110> compression axis) exhibited 80% of walls below 5° and almost none above 10° [24,40]. Crystals of this type have been shown to resist SRX in annealing after channel die compression [72-74], however the 99.999 + Al did undergo dDRX [24]. Unstable crystals <111>, <112> have about 40% below 5° and 20% above 10° [24,40]; the splitting of pole figure orientation indicates formation of DB. These distributions are very similar to those of polycrystals strained at 0.9 and 1.5 at 400°C (shift to higher ψ as ε rises) [40] and even with warm rolled foil (ε = 1.5) (Figure 6) [61]. These specimens would all undergo SRX upon annealing but only the crystals of 99.999+Al underwent dDRX. These distributions confirm the presence of substructure suitable for creating nuclei but growth is not feasible except when extreme purity endows high boundary mobility. The distribution of Kassner and McMahon [44,70] appearing far to the left is based on TEM examination.

Two simple 2-dimensional microstructural models were developed in which a grain 200 μm square divides on straining either at 400°C into 5 μm subgrains (3200 boundary segments) [A1,2] or at 20°C into 1 μm cells (80,000 segments) [68]. The grain boundary length increases as the grains elongate, although the substructure units remain constant in size and number. By ε = 0.2, DB

between deformation bands form [17], about 2 per grain in hot working or 4 per grain in cold working (Figure 2); the DB containing geometrically necessary dislocations increase in length and ψ (10-15° and 12-18° in hot and cold working respectively) (Figure 5). In hot working, the deformation bands do not subdivide because of complete SGB rearrangement in intervals of $\varepsilon \approx \varepsilon_s$ [7-10]. In cold working by $\varepsilon = 0.7$, microbands divide the cells into blocks (10x10) [9,10,19,53-57]; such block walls (BW, 6-9°) become permanent like DB. Initially amounting to about 10% of the cell segments they increase to 15% ($\varepsilon = 1.4$) and 20% ($\varepsilon = 2.1$) as the blocks are kept with maximum dimension of 10 cells in the elongating direction. At both temperatures there is a rising number of permanent high angle boundary segments leaving a reduced number of cell walls ranging between 0.4 and 4° in hot work and 0.5 and 5° for cold work. This continues to a strain of 2.8 in hot working where the grains are only 3w thick; beyond that ε, pinching-off of GB through gDRX keeps the GB area constant [7,9,10,43-46]. In cold working at $\varepsilon = 3.5$, the conversion of DB and BW into layer bands (LB), which are equivalent to GB, results in layers slightly more than one cell thick. Subsequently plastic flow causes the almost unserrated GB to collapse at their sharp triple junctions which migrate so as to zip up the Y and keep the layers constant in thickness and high angle GB area constant [75].

The above high T model, that was set up in conformity with current TEM and HVEM microstructural observations and theories of creep and hot working [7-11,20-22] does not immediately agree with the experimental ones because of the omission of boundaries less than 1° which may amount to 30-50% [24,40,41,61]. Moreover, the distributions do not give any evidence of the type or provenance of the boundaries which was an important aspect of the models. The model agrees with the TEM observations of Kassner and McMahon [70] and of incidental dislocation boundaries (IDB) by Hughes et al [71], who also reported the complementary geometrically necessary boundaries (GNB) similar to the SEM polycrystal distributions (Figures 4,5). When the polycrystal results of Gourdet [40] were moved upwards by adding 30 low ψ walls (<1°) per 100 that distribution came close to the model. One may therefore conclude that in hot

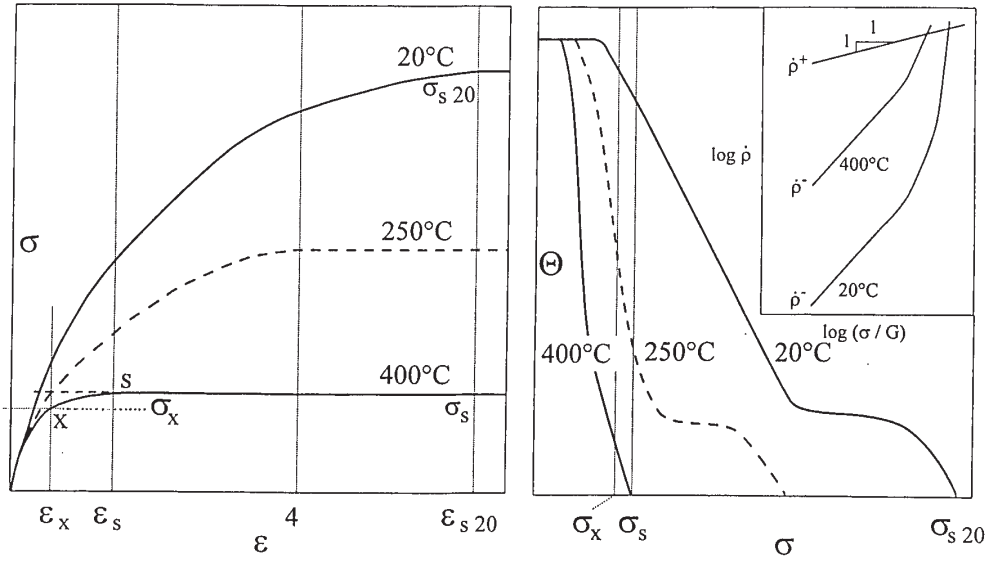

Figure 3. Schematic diagrams illustrating effects of DRV: (a) $\sigma - \varepsilon$, (b) $\theta - \sigma$ and (c) $\log \dot{\rho} - \log (\sigma / G)$ for 400 and 20°C at $\dot{\varepsilon} = 1s^{-1}$ illustrating the disparate conditions for steady state.

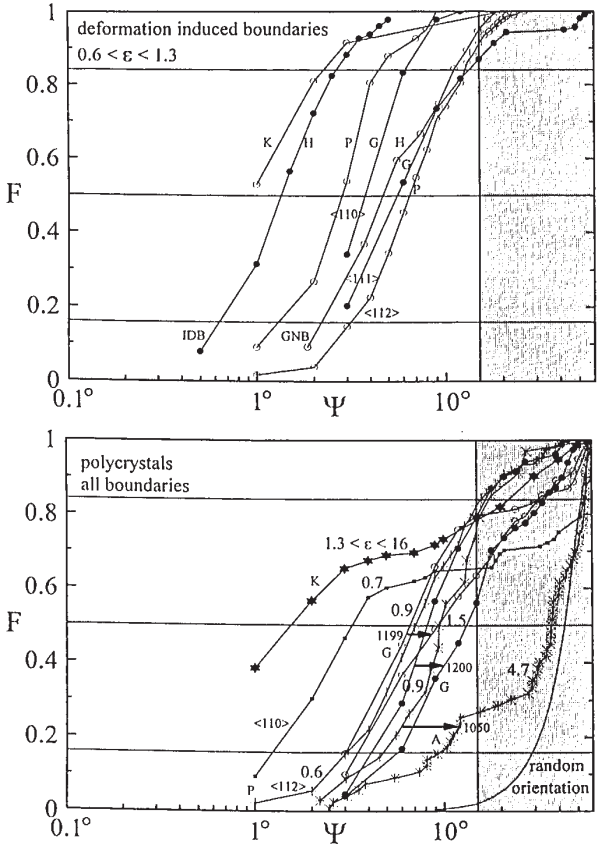

Figure 4. Cumulative frequency F of misorientations ψ of deformation induced boundaries in Al (a) for $\varepsilon \approx 0.7$ in polycrystals (K, 370°C [70]; H, 25°C [71]) and single crystals oriented in <110>, <111> and <112> directions (P, 260°C 99.999+Al [24]; G, 380°C [40]) (measured in sections parallel to compression axis by TEM (K,H,A) and SEM-EBS1 (P,G)). (b) As in (a), but for all boundaries in 1050, 1199 and 1200 Al [40] (thick arrows indicate shift with rising ε), in initially single crystals <110> and <112> [24] and in rolled foil (A, [61]).

working it is the DB or the initial GB which provide nucleation sites; however, these sites are not activated dynamically because DRV either continually rearranges the substructure or reduces the differential energy needed for growth.

Superimposed on the strain hardening and DRV, and independent of temperature, are the Taylor requirements for 3 dominant and 2 limited slip systems in each grain to meet the applied macroscopic shape change [9,10,17-19,32,53-57]. Each of 12 broad initial grain orientations lead to a different set of slip systems with several symmetrically equivalent possibilities one of which is defined by local instabilities or stress concentrations from slip of neighboring grains. In consequence at low ε (~0.1) the grains break up into deformation bands which rotate in different directions defined by their slip systems creating disorientation walls of increasing ψ and persistence [9,10,17,18]. The bands are usually larger (less per grain) in hot working due to constraint reduction by GB sliding and diffusional flow [10]. With further ε, additional rotation in the bands leads to new slip systems. In steady state at 400°C, the ability of the substructure to be completely replaced in $\Delta\varepsilon(< \varepsilon_s)$ permits incidental SGB of the new system to develop without subdivision of the bands (which contain about 10 subgrains across)[7-10] (Figure 2). However, at

20°C in the long transient in which there is little chance of wholesale substructure rearrangement, the new system leads to microshear bands which subdivide the bands into blocks of about 10 cells across; later the microbands (blockwalls) increase in dislocation density and in ψ, becoming persistent [7,10,19,53-57]. During rolling, initial GB, disorientation boundaries and blockwalls rotate towards the rolling plane and become layer bands with a terminal thickness of 1 or 2 cells (Figure 6) separating regions of different orientation as defined by Taylor theory [32,53-57].

4. STATIC RECOVERY AND RECRYSTALLIZATION

Static recovery (SRV) takes place by the same unit mechanisms as DRV but is driven only by internal stress of the substructure; hence at constant annealing T_a the rate rises as T_d declines or ε and $\dot{\varepsilon}$ increase [21,23]. The initial high rate drops exponentially but the progress may be truncated by SRX [1]. An SRV anneal is seldom applied industrially even though it marginally raises the drawability [1,76]. Nevertheless, it always occurs before a planned SRX so that a prolonged heat up may degrade nucleation sites leading to an unexpectedly large grain size. The annealing texture may be altered since potential nucleation sites of different orientations may recover at different rates altering their relative formation and growth rates. In cold drawn conductors (Al-0.65 Fe), a final SRV anneal raises ductility to meet specifications while maintaining suitable strength and long term stability [21,51,77,78]. In multistage rolling and forging, SRV commonly occurs between stages tending to reduce the reloading stresses by about 30% in 20s, substantially countering the increase due to the cooling during the delays [79-83].

Static recrystallization (SRX) in annealing after cold working is widely employed for grain refinement in order to raise both strength and ductility, avoid exfoliation corrosion and particularly develop superplastic properties [1-3,21,58]. Grain size reduction is enhanced by higher ε (higher $\dot{\varepsilon}$, lower T in HW), by inclusion of sufficient density either of large constituent particles (>0.6 μm) to stimulate nucleation or of fine dispersoid particles to restrict grain growth and by addition of suitable solute to raise the strain energy (Mg > 1% to overcome segregation reductions in GB mobility) [1-3,21]. While bulging of existing GB provide nuclei after low ε, SRX nucleates at high ε from about 1 cell in 20 usually in regions of high dislocation density, e.g., through the SRV growth of a cell in a ψ gradient [3,7,12,13,14]. In addition to developing a mobile high ψ boundary, there is need of a suitable internal/matrix strain energy differential. In heavily rolled

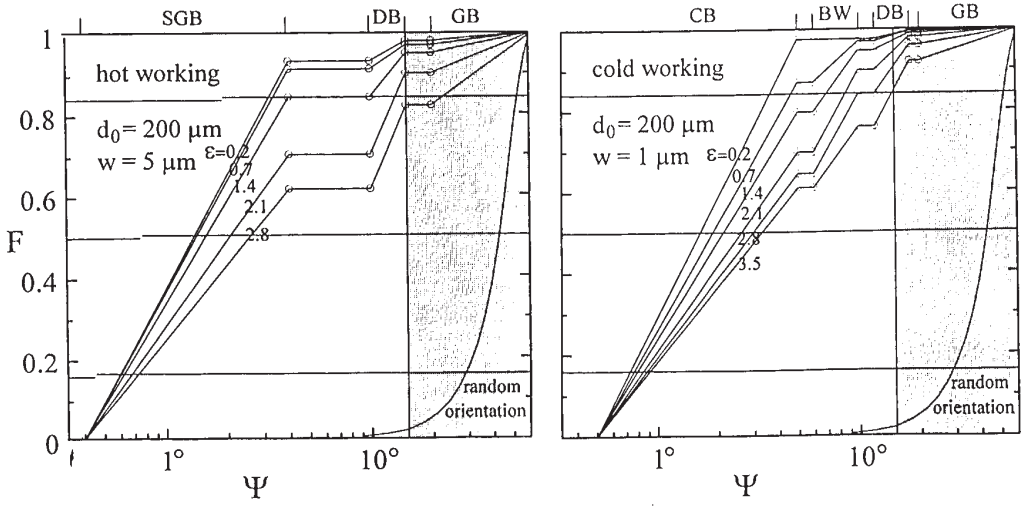

Figure 5. Distributions of boundary segments in microstructural models generated by straining to ε = 0.2, 07, 1.4, .., 3.5: (a) hot working with SGB (0.4 - 4.0), disorientation boundaries DB (10-15°) and GB (20-63°) and (b) cold working with cell walls CW (0.5 - 5°) 4 blockwalls BW (6-9°), DB (12-18°) and GB (20-63°).

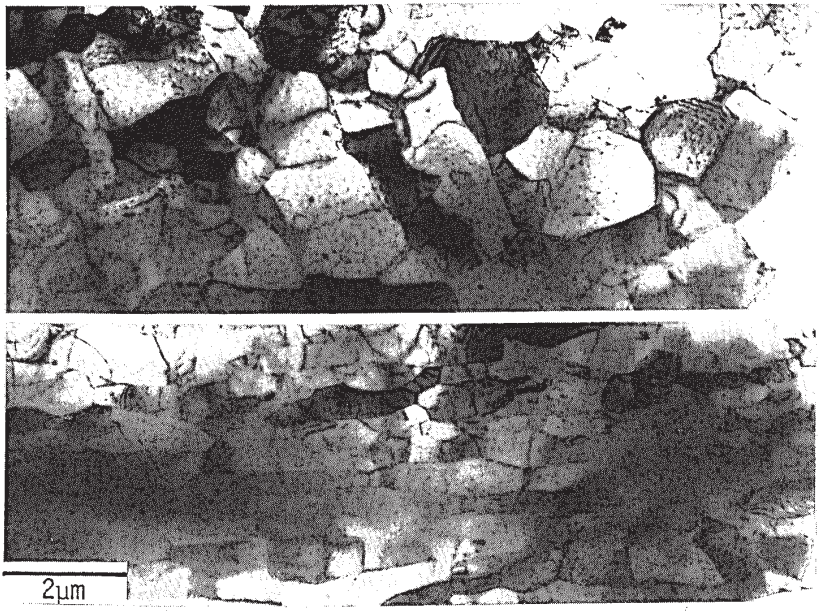

Figure 6. TEM substructure in commercially rolled 1050 Al foil viewed in TD direction: (a) ε=1.5 equiaxed cell structure with serrated DB or GB somewhat discernible near top and bottom; and (b) ε=4.7 (full thickness of foil) layers 1-2cells thick created by blockwalls, DB or GB rotated into rolling plane [61].

plate, SRX nuclei form preferentially from layer bands with the largest cells and largest interlayer ψ and grow rapidly into neighboring layers with smaller cells [32]. This explains why the relatively minor rolling cube component becomes the significant component in the SRX texture. In PSN, the random SRX component is strengthened because the fine cells surrounding the particles do not share the possible Taylor components [34,58,84]. The very different rolling and SRX textures have marked effects on deep drawing causing the location of ears to rotate by 45° relative to the RD. Stated simplistically, it is possible to produce planar isotropic sheet by introducing partial SRX at an intermediate stage of the rolling schedule thus creating a mixed texture [10,84].

In multistage rolling schedules, with T declining from about 500 to 280°C, SRX between stages (1 - i.-.n) is likely to occur after the initial passes when the temperature is high; however, low initial pass strains may require several passes to build up sufficient strain energy [3,80-84]. The guidelines for a schedule to refine the grain size are that the rate of SRX increases and the grain size decreases as ε_i and $\dot{\varepsilon}_i$ increase and as T_i in the pass decreases but the amount of SRX decreases with decreasing interval t_i and $T_{ti} < T_i$. The occurrence of SRX in an interval results in a much softer subsequent pass than that effected by SRV [3,81-83]. Frequent occurrence of SRX after intermediate stages reduce the intensity of the rolling texture and final SRX texture [3,84]. Because of strain accumulation in the final cool passes, coiling above 270°C enhances final SRX with a marked drop in hardness [1].

Alloying has strong and diverse effects on deformation and DRV but its influence on SRX are even more complex. While high concentration of fine particles stabilize substructure raising σ, they also retard SRX and influence texture [21,77,78,82,83]. Large particles (>0.6 μm) raise strain hardening and stimulate nucleation but not after hot working in Mg-free alloys, due to high DRV [3,21,34], the variation in effective PSN changes the proportion of cube and random components in SRX texture [84]. Mg solute reduces DRV, exerting a drag on dislocations so that σ and w^{-1} are about 4 times that of Al [21,22,39,46-48]. It also creates an inverse transient (along with stress exponent of 3) so that the initial stress is defined by separating dislocations from atmospheres

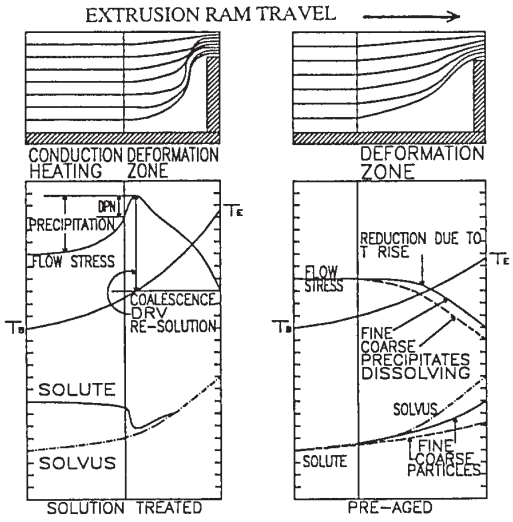

Figure 7. Schematic of effects of (a) prior solution or (b) controlled precipitation treatments. The values of R, V and T_B are the same but T_E is higher for the solutioned than the precipitated. The deformation zone is shorter for the solutioned, because of higher yield and T_E; the lower T_E of precipitated helps avoid failure. The solutioned has a marked rise in stress at the start of deformation due to DPN, but as the particles coalesce and re-dissolve with rising T, the stress drops rapidly to a similar level as the precipitated [6].

[7,11,22,39,46,47] in multistage rolling. This defines the pass flow curve rather than the SRV substructure retained from earlier passes [80,81]. Because it delays alteration of w and s upon change of Z, so that about twice the $\Delta\varepsilon$ is needed compared to that for the $\Delta\sigma$, the SRX nucleation may be controlled by the Z behavior that defined w and s rather than the current Z defining σ; SRX behavior becomes dependent on Z and mode history [3,85,86]. Mg above 2% increases the rate of SRX so that it occurs in schedules with low finishing T or short intervals and alters texture due to multiple stages of SRX and enhanced PSN which is absent in hot working of Mg-free alloys [84].

5. HOT BILLET EXTRUSION

Direct press extrusion of Al alloys with a flat face die is remarkable in producing a semifinished product with a good surface because chamber friction and die dead zone trap the oxidized billet surface [4-6,28,87,88]. The flat face die produces a limited deformation zone with severe radial ε and $\dot{\varepsilon}$ gradients so that central regions reach steady state but peripheral regions strain harden severely. This gives rise to a positive mean stress at the die aperture (despite the high compressive stress in the chamber) which can easily initiate cracks at segregated particles that range from hard to molten (eutectic) [5,6,28,87-90]. The intense deformation in the zone leads to a rise of 50 to 100°C which causes the substructure in each longitudinal fiber to progressively rearrange from a dense to a more recovered state; this is countered by a rise in $\dot{\varepsilon}$ which is more marked towards the surface [5,6,28,88-90]. In the most intensely deformed zones, DRX has been observed in Al-5Mg-Mn and in Al-7Mg [5,28-31,34,39]. The expected rise limits the billet preheat to 350-400°C to keep final T_E below incipient melting that is usually lower for harder alloys. However, the preheat T_B must be selected in relation to the extrusion ratio R to yield a breakout pressure below the press capacity. The pressure shows an initial sharp drop as the deformation zone heats up and then declines slowly with decreasing chamber friction [4,28,87-90]. The ram speed V_R must be controlled to limit the T rise to prevent surface defects.

In all alloys, a major objective is homogenization to eliminate eutectic zones to reduce the size of particles converting them to less damaging types and to distribute the alloying elements uniformly [5,28,88]. Problems of segregation are generally worse in the 5XXX, 2XXX and 7XXX alloys which have considerably higher solute and hence hot strength than the 6XXX or 700X (no Cu) alloys which have good extrudability [4-6,28,87]. For precipitation alloys, the softest form produced by stepped cooling of billets has overaged (medium size) precipitates which least constrain the dynamic recovery. However, if billets are cooled directly from homogenization (where the alloying elements are in solution) to T_B, there is a possibility of dynamic precipitation in the billet which drastically reduces the DRV and greatly adds to the initial pressure although it does avoid large particles that cause surface cracking [6,91]. An industrially useful procedure for the 6XXX and 700X alloys is press heat treatment in which medium-fine, uniformly-distributed particles are dissolved in the extrusion hot zone (Figure 7) [6,28,91]. Because of their low quench sensitivity, it is possible to keep the elements in solution by air jet cooling causing only limited distortion that is easily removed by stretching; cooling at the die exit avoids the need of long solution furnaces and quench tanks. The hotwork dislocation substructures in 6XXX and 700X results in more uniform precipitation and properties that match those from normal heat treatment [6]. The 2XXX and 7XXX alloys cannot be easily press heat treated because high quench sensitivity requires cooling rates that cause severe distortion difficult to correct; moreover, the 7XXX precipitation is adversely affected by the dislocation substructure, failing to produce suitable combinations of strength, toughness and resistance to fatigue and corrosion [58,91,92]. The substructures produced in extrusion have the same relationship to T, $\dot{\varepsilon}$, Z and σ as in simple hot working tests; however, there is a severe radial gradient in level of DRV, declining toward the surface [5,6,28,31,87,88,93]. The retention of the hot work substructure can easily be achieved by industrial cooling techniques at the press exit. The additional product strength is a great benefit particularly in non-heat treatable alloys such as 3XXX, 5XXX series and in the lean precipitate 6XXX and 700X alloys. The strength is also increased by the <111> and <110> texture; the <111> component is stronger at lower T while <100> prevails at higher T [9,58,93,94]. The more distorted <111> regions recrystallize more quickly to a similar texture. Removal, even to a limited extent during secondary fabrication, of the stronger layer near the surface or in thinner sections (which raise the average section strength) can create problems. Furthermore, there is the problem that SRX may occur during inadequate cooling or subsequent heating in fabrication; here also, it is the stronger regions that are softened leaving disproportionally adverse effects. Moreover while the less recovered surface results in reasonably fine grains, the highly recovered interior may produce very large grains which also markedly detract from the properties [5,28,31,87,88,95]. In cases where SRX occurs, as during solution treatment of the 2XXX and 7XXX alloys, the entire processing and particle additions must be controlled to provide suitable grain size [28,87,88].

6. HOT AND WARM ROLLING

Flat rolling is a significant technology not only for the tonnage produced but in so far as the texture and grain size of the sheet are of great significance for subsequent forming. In beverage can production it is very important to develop planar isotropy so that deep drawing does not develop ears and ironing is enhanced. Hot rolling on cold rolls develops T gradients and thus strain energy decreasing from surface to center which tends to produce a gradient of SRX nucleation rate (fine to large grains). Industrial rolling is usually conducted in a multistage schedule (~12 passes, 500 - 300°C) so that some SRX occurs only after the early stages; interpass SRV becomes more prevalent but less effective with diminished T, causing strain energy to accumulate across the stages. The mean pass stresses increase throughout the schedule at an intermediate rate between those for SRX materials entering each pass and those for instantaneous reloading as calculated from the drop in T [80-83,96,97]. In contrast to extrusion, the straining progresses from hot to warm with SRV between passes; during each pass the pre-existing substructure must undergo a change to a smaller wall spacing causing a higher initial stress but lower strain hardening. Furthermore, incipient melting is a possible problem near the centerline in the early passes and cracking at cold barreled edges in the final ones.

The rolling of slabs to strip is progressively closer to plane strain conditions. The frictional forces pulling the materials into the rolls and retarding its exit after the neutral point (slab and roll velocity equal) result in a decreasing shear strain gradient from surface inward which is partially reversed in traversing the entire arc of contact [98]. In calculating the texture from the basic Taylor theory with possible modern modifications, it is necessary to take into account the shear rotations as well as the grain elongations. The model starts with the random or measured texture of the slab and applies the possible Taylor rotations to the various orientations. In general there must be 5 slip systems operating per grain, although 2 may be rather minor. The alternatives in the Taylor theory account in part for the formation of deformation bands which rotate in symmetrical manners (Figure 2). The size of the grains (as long as there are many) or the degree of break up is not important to the texture calculation; however, additional deformation modes at elevated temperature can alter the texture to some degree. The presence of large particles which produce turbulent flow gives rise to additional orientations [84,99,100]. In multistage schedules in which SRX takes place at a particular interval, the texture calculation must commence anew for those grains taking account of their texture.

The macrotexture consists of distinct components, each of which represents the orientations of a group of cells [53-57]. The distributions of the groups are dependent on the scale of the mechanisms creating high misorientation boundaries. The rolling textures in hot and cold working contain the same components and the recrystallization textures are also similar, yet the rates and grain sizes of SRX are different. There is strong evidence that in the layered cold worked microstructure (Figure 6), the cube layer cells are larger and more recovered than other orientations so that they become nuclei and grow preferentially [32,84]. Cube oriented subgrains in hot worked materials must have similar advantage yet there are sufficient differences that additional new explanation is needed. Recrystallization texture is described in Section 5. In Al the rolling texture at both center and surface do not alter substantially as T rises from cold to hot; however, the cubic component is usually higher as T rises [1,98]. Generally, the SRX texture is cube type after both hot and cold rolling; however, random components appear if PSN occurs (only in Mg alloys after hot working) [84,98-100].

7. CONCLUSIONS

Dynamic recovery is an integral part of the deformation process across the hot, warm and cold working ranges, with a decrease in the scale of substructure produced and an associated increase in stress as temperature decreases and strain rate rises. It interacts with the Taylor polycrystal constraints to change the scale of the microtexture substantially with little change in macrotexture. In producing markedly different texture, recrystallization is a starkly different mechanism from those of deformation and recovery, yet dependent on them for its scale and rate. Due to high levels of dynamic recovery, dynamic recrystallization takes place only under limited circumstances. Dynamic recovery and static recrystallization can be manipulated in quite different combinations in primary processes such as extrusion and rolling, as a result of the dissimilar intensities and rates of strain and temperature variation. The diverse effects of solutes and different particle sizes on strain hardening and DRV are made more complex by their varied influence on static recrystallization.

Acknowledgments The authors wish to express appreciation for support from the Alexander von Humboldt Foundation, NSERC (Canada), FCAR (Québec) and DFG (Germany).

REFERENCES

1. G.M. Raynaud, B. Grange and C. Sigli, Al Alloys, Physical Mechanical Properties, ICAA3, L. Arnberg et al., eds. NTH, SINTEFF, Trondheim, (1992), pp 169-214.
2. G.J. Marshall, (ICAA5), Mat.Sci. Forum, 217-222, (1996), 19-30.
3. H.J. McQueen, 'Hot Rolling of Al Alloys', Hot Deformation of Al Alloys, T.R. Bieler et al., eds, TMS-AIME Warrendale PA (1998) (in press).
4. H.J. McQueen and O.C. Celliers, Materials Forum (Australia), 17, (1993), 1-13.
5. H.J.McQueen and O.C.Celliers, Can.Metal.Quart., 35, (1996), 305-319.

6. H.J. McQueen and O.C. Celliers, Can. Metal. Quart., 36, (1997), pp. 73-86.
7. W. Blum and H.J. McQueen, Aluminum Alloys, Physical and Mechanical Properties, (ICAA5) J.H. Driver et al., eds. Mat.Sci. Forum, 217-222, (1996), 31-42.
8. W. Blum, Q. Zhu, R. Merkel and H.J. McQueen, Al Alloys, Physical Mechanical Properties, (ICAA5, J.H. Driver et al., eds., Transtech Pub., Switz.), Mat.Sci.Forum, 217-222, (1996), 611-616.
9. H.J. McQueen, 'The Hot Worked State', (Section 9 'Current Issues in Recrystallization: A Review', Mat. Sci. Eng., 238, (1998), pp. 219-274.
10. H.J. McQueen and W. Blum, Recrystallization and Related Topics (Proc. 3rd Intnl. Conf., ReX '96), T.R. McNelley, ed., Monterey Inst. Advanced Studies, CA, (1997), pp. 123-136.
11. W. Blum, Hot Deformation of Al Alloys, T.G. Langdon et al., eds., (TMS-AIME Warrendale, PA, 1991), pp. 181-210.
12. F.J. Humphreys and M. Hatherley, Recrystallization and Related Annealing Phenomena, (Pergamon Press, Oxford 1995).
13. R.D. Doherty, D.A. Hughes, F.J. Humphreys, J.J. Jonas, D. Juul-Jansen, M.E. Kassner (editor) W.E. King, T.R. McNelley, H.J. McQueen and A.D. Rollett), Mat. Sci. Eng., 238, (1998), pp. 219-274.
14. H.J. McQueen, E. Evangelista, N. Jin, M.E. Kassner, (see reference 22), pp. 251-266.
15. H.J. McQueen, E. Evangelista, and M.E. Kassner, Z. Metallkde., 82, (1991), 336-345.
16. H.J. McQueen, E. Evangelista and N.D. Ryan, Recrystallization ('90) in Metals and Materials, T. Chandra, ed., (AIME, Warrendale, PA 1990), pp. 89-100.
17. C.S. Barrett and L.H. Levenson, Trans.AIME, 137, (1990), 112-127.
18. M. Hatherley, Strength of Metals and Alloys (ICSMA6), R.C. Gifkins ed., (Pergamon Press, Oxford 1982), 3, pp. 1181-1195.
19. M. Richert and H.J. McQueen, Hot Workability of Steels and Light Alloys-Composites, H.J. McQueen, E.V. Konopleva, N.D. Ryan, eds., (Met. Soc. CIM, Montreal 1996), pp. 15-26.
20. H.J. McQueen, Mat. Sci. Eng., A101, (1987), 149-160.
21. H.J. McQueen, Hot Deformaton of Aluminum Alloys, T.G. Langdon, H.D. Merchant, eds., (TMS-AIME, Warrendale, PA 1991), pp. 31-54.
22. H.J. McQueen, W. Blum, Q. Zhu and V. Demuth, Advances in Hot Deformation Textures and Microstructures, J.J. Jonas, T.R. Bieler, KJ. Bowman, eds., TMS-AIME, Warrendale, P.A., (1993), pp. 235-250.
23. T. Hasegawa, T. Yakou and U.F. Kocks, Acta Metal, 30, (1982), 235; 27, (1979), 1705.
24. D. Ponge, M. Bredehoft and G. Gottstein, Scripta Mater., 37, (1997), 1769-1775.
25. M.E. Kassner, H.J. McQueen, J. Pollard, E. Evangelista and E. Cerri, Scripta Metal. Mat., 31, (1994), 1331-1336.
26. H. Yamagata, Scripta Metal.Mat., 30, (1994), 411-416.
27. Y. Huang and F.J. Humphreys, Thermac '97, T. Chandra, T. Sakai, eds., TMS AIME Warrendale, PA., (1997), pp. 987-993.
28. T. Sheppard, M.G. Tutcher and H.M. Flower, Met. Sci., 13, (1979), 473-481.
29. T.Sheppard, M.A.Zaidi, M.G.Tutcher and N.C.Parson, Microstructural Control in Al Alloy Processing, H.Chia and H.J.McQueen,eds.,TMS-AIME,Warrendale PA (1985), pp.155-178.
30. T. Sheppard, N.C. Parson and M.A. Zaidi, Met. Sci., 71, (1983), 481-490.
31. T. Sheppard and M.G. Tutcher, Met. Tech., 8, (1981), 319-327.
32. E. Nes, H.E. Vatne, O. Daaland, T. Furu, R. Orsund, K. Marthinsen, Aluminum Alloys Physical and Mechanical Properties (ICAA4), T. Sanders, E. A. Starke, eds., (Georgia Inst. Tech., Atlanta 1994), 2, pp. 250-257.
33. T. Sakai and J.J. Jonas, Acta Metall., 32, (1984), 189-209.
34. F.J. Humphreys and P. Kalu, Acta Metal., 35, (1987), 2815-2829.
35. S.J. Hales, T.R. McNelley and H.J. McQueen, Metal. Trans., 22A, (1991), 1037-1047.
36. D.B. Brooks, H. Gudmundsen and J.A. Wert, (see reference 21), pp. 55-58.
37. B.M.Watts,M.J.Stowell,B.L.Baikie and D.G.Owen,Met. Sci.,10, (1976), 189-197,198-205.
38. F.R. Castro-Fernandez and C.M. Sellars, Mat. Sci. Tech., 4, (1988), 621-627.
39. H.J. McQueen and M.E. Kassner, Superplasticity in Aerospace II., T.T McNelley, H.C. Herkkenen, eds., (TMS-AIME, 1991), pp. 189-206.
40. S. Gourdet, 'Etude des Mecanismes de Recristallisation au Cours de la Deformation à Chaud de Al.', Ph.D. Thesis, Ecole National Superior des Mines de Saint Etienne, France, (1997).
41. S.Gourdet, E.V.Konopleva, H.J.McQueen and F. Montheillet, (see reference 23), 441-446.
42. H. Ahlborn, E. Hornbogen and U. Koster, J. Mat.Sci., 4, (1969), 944-950.

43. J.K.Solberg, H.J. McQueen, N.Ryum and E. Nes, Phil. Mag. 60 (1989), 447-471; 473-485.
44. M.E. Kassner and M.E. McMahon, Met. Trans., 18A, (1987), 835-846.
45. M.E. Kassner, M.M. Myshlyaev and H.J. McQueen, Mat. Sci. Eng., A108, (1989), 45-61.
46. W. Blum, Q. Zhu, R. Merkel and H.J. McQueen, Z. Metalkde, 87, (1996), 341-348.
47. W. Blum, Q. Zhu, R.Merkel and H.J. McQueen, Mat. Sci. Eng., A205, (1996), 23-30.
48. G.A. Henshall, M.E. Kassner and H.J. McQueen, Metal. Trans., 23A, (1992), 881-889.
49. M.R. Drury and F.J. Humphreys, Acta Met., 34, (1986), 2259-2271.
50. B. Verlinden, Catholic University, Leuven, Belgium (personal communication).
51. E.V. Konopleva, H.J. McQueen and W. Blum, Microstructural Sci., 22, (1995), 297-314.
52. H.J.McQueen, W.Blum, S.Straub, M.E.Kassner, Scripta Metal Mat., 28, (1993) 1299-1304.
53. D.A. Hughes, Al Alloys for Packaging II, J. Morris et al., eds., (TMS-AIME Warrendale PA, 1996), 129-144.
54. B.Bay, N.Hansen, D.A.Hughes, D.Kuhlman-Wilsdorf, Acta.Metal.Mat,.40 (1992) 205-219.
55. D.A. Hughes and N. Hansen, Advances in Hot Deformation Textures and Microstructures, J.J. Jonas et al., eds., (TMS-AIME, Warrendale, PA 1995), pp. 427-444.
56. N.Hansen and D. Juul-Jensen, Hot Working of Al Alloys, T.G. Langdon et al., eds. (TMS AIME Warrendale PA 1991), pp. 3-20.
57. D.A. Hughes and Y.L. Liu, ibid, pp. 21-30.
58. H.J. McQueen and J.J. Jonas, Aluminum Alloys '90, ICAA2, C.Q. Chen, ed., (Beijing, 1990), pp. 727-742.
59. W. Blum, Plastic Deformation and Fracture of Materials, H. Mughrabi, ed., VCH Weinheim, (1993), pp. 359-405.
60. W. Blum, The Johannes Weertman Symposium, R.W. Arsenault et at., eds., TMS-AIME, Warrendale, PA (1996), pp 103-117.
61. M. Abral and W. Blum, Al Alloys, Physical Mechanical Properties, ICAA6, Japan, (1998).
62. K. Marthinsen and E. Nes, (ICSMA11), Mat.Sci. Eng., A234-236, (1997), 1095-1098.
63. E. Nes, Al Alloys, Physical Mechanical Properties, ICAA6, Japan, (1998).
64. M. Meier, Q. Zhu and W. Blum, Z. Metallkde., 84, (1993), 263.
65. Q. Zhu and W. Blum, Aspects of High Temperature Deformation and Fracture in Crystalline Materials, Y. Husui et al., eds., JIMIS-7, (1993), 649-656.
66. I. Poschmann and H.J. McQueen, Physica Status Solidi, A149, (1995), 341-348.
67. I. Poschmann and H.J. McQueen, Scripta Metal. Mat., 35, (1996), 1123-1128.
68. F. Schuh and M. Von Heimendahl, Z. Metallkde, 65, (1974), 346.
69. Ch. Perdrix, M.Y. Perrin and F. Montheillet, Mem. Et.Sci.Rev. Métal., 78, (1981), 309-320.
70. M.E. Kassner and M.E. McMahon, Creep and Fracture of Engineering Materials and Structures, B. Wilshire, R.W. Evans, eds., Inst. Metals, London, (1987), pp. 29-40.
71. D.A. Hughes, Q. Liu, D.C. Chrzan and N. Hansen, Acta Mater., 45, (1997), 105-112.
72. C.L. Maurice, M.C. Theyssier and J.H. Driver, Advances in Hot Deformation Textures and Microstructures, J.J. Jonas et al., eds., (TMS-AIME, Warrendale, PA 1995), pp. 411-425.
73. J.H. Driver, Microstructural and Crystallographic Aspects of Recrystallization, N. Hansen et al. eds. (Riso Natl. Lab, Roskilde, DK 1995), pp. 25-36.
74. M.C.Theyssier,B.Chenal,J.H.Driver,N.Hansen, Phys.Stat.Sol., Al49, (1995), pp. 367-378.
75. H.J. McQueen and S. Gourdet, 'Varieties and Limitations of Dynamic Recrystallization Mechanisms in Al Alloys', Scripta Mater, 38, (1998), (submitted).
76. R. Grimes and J.C. Wright, J. Inst. Met., 96, (1968), 182-186.
77. H.J. McQueen, J. Mat. Proc. Tech., 37, (1993), 3-36.
78. H.J. McQueen, H. Chia and E.A. Starke, Microstructural control in Al Alloy Processing, H. Chia, H.J. McQueen, eds., TMS-AIME, Warrendale, PA, (1985), pp. 1-18.
79. H.J. McQueen, G. Avramovic-Cingara, K. Conrod, Can.Metal.Quart., 32, (1993), 375-386.
80. I. Poschmann and H.J. McQueen, Z. Metallkde., 87, (1996), 349-356.
81. I. Poschmann and H.J. McQueen, Z. Metallkde., 88, (1997), 14-22.
82. H.J. McQueen, G. Avramovic-Cingara, P. Sakaris and A. Cingara, Proc. 3rd Intnl. SAMPE Metals Conf., (Toronto), (1992), pp. M192-M206.
83. G. Avramovic-Cingara, K. Conrod, A. Cingara and H.J. McQueen, Light Metals Processing and Applications, Met. Soc. CIMM, Montreal, (1993), pp. 495-510.
84. J. Hirsch, Thermec 97, T. Chandra, T. Sakai, eds., TMS-AIME, Warrendale, PA., (1997), pp. 1083-1094.
85. G.J. Baxter, T. Furu, J.A. Whiteman and C.M. Sellars, (ICAA5), Mat. Sci. Forum, 217-222, (1996), 459-464.

86. C.M. Sellars, Recrystallization and Related Phenomena, (Proc. ReX'96), T. McNelley, ed., Monterey Inst. Advanced Study (1997), pp. 81-94, (with Q. Zhu), pp. 195-202.
87. T. Sheppard, Proc. 8th Light Metal Congress, J. Jeglitsch et al., eds., The University, Leoben, (1987), pp. 301-311.
88. T. Sheppard, S.J. Paterson and M.G. Tutcher, Microstructural Control in Al Alloys, E.H. Chia, H.J. McQueen, eds., Met. Soc. AIME, Warrendale, PA, (1986), pp. 123-154.
89. E. Herba and H.J. McQueen, Al Alloys, Physical, Mechanical Properties, (ICAA6), T. Sato, ed., Japan (1998).
90. M. Sauerborn and H.J. McQueen, Mat. Sci. Tech., (1998), (in press).
91. H.J. McQueen, Hot Deformation of Aluminum Alloys, T.G. Langdon et al., eds., Met. Soc. AIME, Warrendale, PA, (1991), pp. 105-120.
92. E.A. Starke, and J.C. Williams, Deformation, Processing and Structure, G. Krausz, ed., ASM, Metals Park, Ohio, (1984), pp. 279-354.
93. A. Plumtree and G. Deep, Met. Tech., 4, (1977), 1-5.
94. E. Hirosowa, J. Japan Inst. Met 92, (1963), 78-81.
95. S.J. Paterson and T. Sheppard, Met. Tech., 9, (1982), 389-398.
96. E. Evangelista, H.J. McQueen, N.D. Ryan and J. Bowles, Stainless Steels, 1991 (Chiba), Iron Steel Inst. Japan, Tokyo, (1991), pp. 842-849.
97. N.D. Ryan and H.J. McQueen, J.Mat.Proc. Tech., 36, (1993), 103-123.
98. H.J. McQueen and H. Mecking, Z. Metallkde, 78, (1987), 387-395.
99. J. Hirsch, K. Karhausen and R. Kopp, Al Alloys, Physical, Mechanical Properties, (ICAA4), T. Sanders, E.A. Starke, eds., Georgia Inst. Tech., Atlanta (1994), pp. 476-483.
100. J. Hirsch, (see reference 21), pp. 379-389.